SOIL Discuss., https://doi.org/10.5194/soil-2019-28
Manuscript under review for journal SOIL
Discussion started: 22 May 2019

Time-lapse monitoring of root water uptake using electrical resistivity tomography and Mise-à-la-Masse: a vineyard infiltration experiment

Benjamin Mary[1], Luca Peruzzo[2,3], Jacopo Boaga[1], Nicola Cenni[1], Myriam Schmutz[3], Yuxin Wu[2], Susan S. Hubbard[2], Giorgio Cassiani[1]

[1]Dipartimento di Geoscienze, Università degli Studi di Padova, Via G. Gradenigo, 6–35131 Padova, Italy
[2]Earth and Environmental Sciences Area, Lawrence Berkeley National Laboratory, 1 Cyclotron Rd, Berkeley, CA, 94720, USA.
[3]EA G&E 4592, Bordeaux INP, University Bordeaux Montaigne, 1 allée Daguin, 33607 Pessac, France

Correspondence to: Benjamin Mary (benjamin.mary@unipd.it)

Abstract. This paper presents a time-lapse application of electrical methods (Electrical Resistivity Tomography – ERT – and Mise-à-la-Masse – MALM) for monitoring plant roots and their activity (root water uptake) during a controlled infiltration experiment. The use of non-invasive geophysical monitoring is of increasing interest as these techniques provide time-lapse imaging of processes that otherwise can only be measured at few specific spatial locations. The experiment here described was conducted in a vineyard in Bordeaux (France) and was focused on the behaviour of two neighbouring grapevines. The joint application of ERT and MALM has several advantages. While ERT in time-lapse mode is sensitive to changes in soil electrical resistivity and thus to the factors controlling it (mainly soil water content, in this context), MALM uses DC current injected in a tree stem to image where the plant-root system is in effective electrical contact with the soil at locations that are likely to be the same where root water uptake (RWU) takes place. Thus ERT and MALM provide complementary information about the root structure and activity. The experiment shows that the region of likely electrical current sources produced by MALM does not change significantly during the infiltration study time in spite of the strong changes of electrical resistivity caused by changes in soil water content. This fact, together with the evidence that current injection in the soil produces totally different patterns, corroborates the idea that this application of MALM highlights the active root density in the soil. When considering the electrical resistivity changes (as measured by ERT) inside the stationary volume of active roots delineated by MALM, the overall tendency is towards a resistivity increase, which can be linked to a decrease in soil water content caused by root water uptake. On the contrary, when considering the soil volume outside the MALM-derived root water uptake region, the electrical resistivity tends to decrease as an effect of soil water content increase caused by the infiltration. The results are particularly promising, and the method can be applied to a variety of scales including the laboratory scale where direct evidence of roots structure and root water uptake can help corroborate the approach. Once fully validated, the joint use of MALM and ERT can be used as a valuable tool to study the activity of roots under a wide variety of field conditions.

SOIL Discuss., https://doi.org/10.5194/soil-2019-28
Manuscript under review for journal SOIL
Discussion started: 22 May 2019

1 Introduction

The interaction between soil and biota is one of the main mechanisms controlling the exchange of mass and energy between the Earth's terrestrial ecosystems and the atmosphere. Philip (1966) was the first to use the phrase "soil–plant–atmosphere continuum" (SPAC) to conceptualize this interface in the framework of continuum physics. Even though more than five decades have elapsed and many efforts have been expended (e.g., Maxwell et al., 2007; de Arellano et al., 2012; Anderegg et al., 2013; Band et al., 2014), the current mechanistic understanding or modelling of SPAC of SPAC is still unsatisfactory (e.g. Dirmeyer et al., 2006, 2014). This is not totally surprising, since soil-plant interactions are complex, exhibiting scale- and species-dependence with high soil heterogeneity and plant growth plasticity. In this study, we focus on new methods to help understand complex root-soil systems (the rhizosphere, e.g. York et al., 2016).

Roots contribute substantially to carbon sequestration. Roots are the connection between the soil, where water and nutrients reside, to the other organs and tissues of the plant, where these resources are used. Hence roots provide a link in the pathway for fluxes of soil water and other substances through the plant canopy to the atmosphere (e.g. Dawson and Stiegwolf, 2007). These transpiration fluxes are responsible for the largest fraction of water leaving the soil in vegetated systems (Chahine, 1992). Root Water uptake (RWU) influences the water dynamics in the rhizosphere (Couvrer et al., 2012) and the partitioning of net radiation into latent and sensible heat fluxes thereby impacting atmospheric boundary layer dynamics (Maxwell et al., 2007; de Arellano et al., 2012). Yet, a number of issues remain when representing RWU in both hydrological and atmospheric models. Dupuy et al. (2010) summarize the development of root growth models from its origins in the 1970s with simple spatial models (Hackett and Rose, 1972; Gerwitz and Page, 1974) to the development of very complex plant architectural models (Jourdan and Rey, 1997). Dupuy et al. (2010) advocate for a different approach, where roots systems are described as "density" distributions. Attempts in this direction (Dupuy et al., 2005; Draye et al., 2010; Dupuy and Vignes, 2012) require much less specific knowledge of the detailed mechanisms of meristem evolution, and yet are sufficient to describe the root "functions" in the framework of continuum physics, i.e. the one endorsed by the SPAC concept. These models also lend themselves more naturally to calibration against field evidence, as they focus on the "functioning" of roots, especially in terms of RWU (e.g. Volpe et al., 2013, Manoli et al., 2014). However, calibration requires that suitable data are available in a form comparable with the model to be calibrated. This is the main motivation behind the work presented herein.

A thorough understanding of root configuration in space and their evolution in time is impossible to achieve using only traditional invasive methods: this is particularly true for root hairs, i.e. for the absorptive unicellular extensions of epidermal cells of a root. These tiny, hair-like structures function as the major site of water and mineral uptake. Root hairs are extremely delicate, turn over quickly, and are subject to desiccation and easily destroyed. For these reasons, direct investigation of their in situ structure via excavation is practically impossible under field conditions.

The development of non-invasive or minimally invasive techniques are required to overcome the limitations of conventional invasive characterization approaches. Non-invasive methods are based on physical measurements at the boundary of the domain of interest, i.e. at the ground surface and, when possible, in shallow boreholes. Non-invasive methods provide spatially

extensive, high-resolution information that can also be supported by more traditional local and more invasive data such as soil samples, TDR, lysimeters and rhizotron measurements.

In the investigation of roots and RWU the most widely used non-invasive technique is Electrical Resistivity Tomography (ERT – e.g. Binley and Kemna, 2005). ERT measures soil electrical resistivity and, in time-lapse mode, resistivity changes over time. Electrical resistivity values depend on soil type and its porosity, but also on state variables such as the saturation of electrolyte (water) in the pores, and the concentration of solutes in the pore water (as described e.g. by the classical Archie's law, 1942). Note, however, that other factors may play a role, such as clay content (Rhoades et al., 1976; Waxman and Smits, 1968) and temperature (e.g., Campbell et al., 1949). However, in general, it is possible to estimate water content changes from changes in electrical resistivity over time (and space) provided that pore water salinity does not vary dramatically. While ERT has been attempted for quantifying root biomass on herbaceous plants (e.g. Amato et al., 2009), the main use of this technique in this context aims at identifying changes in soil water content in space and evolution in time (e.g., Michot et al., 2003, 2016; Srayeddin and Doussan, 2009; Garré et al., 2011; Cassiani et al., 2012, Brillante et al. 2015). With specific reference to RWU, Cassiani et al. (2015, 2016), Consoli et al. (2017) and Vanella et al. (2018) used time-lapse ERT with 3D cross-hole configurations to monitor changes in soil electrical resistivity caused by irrigation and RWU for different crops (apple and citrus trees). It should also be noted that RWU and the release of different exudates by fine roots modify soil water content and resistivity at several temporal scales (York et al., 2016).

On the other hand, evidence suggests that roots themselves may produce signals in ERT surveys (Amato et al., 2008; Werban et al., 2008); however, these signals are often difficult to separate from soil heterogeneities and soil water content variations in space. Nevertheless, in most cases, the ranges of electrical resistivity of soil and roots overlap, and while the amplitude of contrasts varies according to the soil resistivity and tree species (e.g. Mary et al., 2016), the direct identification of root systems using ERT is often impractical.

Other electrical signals may contribute to the detection of roots and to the characterization of their activities. For instance, self-potential (SP) signals can be associated with plant activities: water uptake generates a water circulation and a mineral segregation at the soil–roots interface that induce ionic concentration gradients which in turn generate voltages of the order of a few mV (Gibert et al., 2006). However, such SP sources are generally too low to be detectable in normally noisy environment. Induced Polarization (e.g. Kemna et al., 2012) is also a promising approach in root monitoring. This is consistent with the fact that root systems are commonly modelled as electrical circuits composed of resistance R and capacitance C (e.g. Dalton, 1995 and similar models). Recently, Mary et al. (2017) considered polarization from soil to root tissues, as well as the polarization processes along and around roots, to explain the phase shift (between injected current and voltage response) observed for different soil water content. Weigand and Kemna (2017, 2019) demonstrated that multi-frequency electrical impedance tomography is capable of imaging root systems extent.

Recently, the Mise-A-La-Masse (MALM) method has been proposed for plant root mapping. MALM is a classical electrical method (Parasnis, 1967) originally developed for mining exploration, but also used more recently e.g. in the context of landfill characterization (De Carlo et al., 2013) as well as conductive tracer test monitoring (Osiensky, 1997; Perri et al., 2018). In

MALM, an electrical current is injected into a conductive body with a return current electrode far away ("at infinity"), and the resulting voltage is measured at the ground surface or in boreholes, again with a reference electrode at infinity: the shape of voltage contour lines is informative about the extent and orientation of the conductive body. This idea can be applied to the plant stem and roots system, considering that electrical current can be transmitted through the xylem and phloem (on either side of the cambium), where sap flow takes place. The main assumption is that fine root connections and mycorrhiza at the contact between roots and soil convey the injected current into the soil where this contact is efficient, thus appearing as a distribution of current sources in the ground. The location of these sources should correspond to the locations of active contacts between roots and soil, and could be identified starting from the measured voltage distribution at the ground surface or in boreholes. This approach has been recently test by Mary et al. (2018) on vine trees, showing that current injection in the stem and in the soil just next to the stem produces very different voltage patterns, thus confirming that the stem-roots system conveys current differently from a direct injection in the ground.

In this study we present the results of an infiltration experiment conducted in a Bordeaux vineyard (France). The experiment was monitored (also) using time-lapse 3D ERT and time-lapse MALM measurements, the latter performed by injecting current in the vine trees stems. This study had the following goals:

(a) define a non-invasive investigation protocol capable of "imaging" the root activity as well as the distribution of active roots, at least in terms of their continuum description mentioned above;
(b) Integrate the geophysical results with mass fluxes measurements in/out of the soil-plant continuum system.

2 Methodology

2.1 Site description

The study was conducted in a commercial vineyard (Chateau La Louviere, Bordeaux) in the Pessac Leognan Appellation of France (long 44°44'15''N, lat 0°34'45''W). The climate of the region is oceanic with a mean annual air temperature of 13.7 °C and about 800 mm annual precipitation. Grapevine trees are planted at 1 m distance along the rows, and the rows are spaced about 1.5 m. We focused our interest on two neighbouring plants.

The vineyard is not irrigated. The soil is sandy down to 1 m depth with sandy clay below, down to 1.75 m, and calcareous at depth. Due to its high porosity, the sandy layer has a relatively poor water retention capacity. Nevertheless, the water supply of the vine plant is not a limiting factor - refer to Mary et al. (2018) for more details about the plants and soil type.

We concentrated our monitoring on only two neighbouring grapevines (Figure 1), which differed in age and size: plant A was smaller and younger, plant B was considerably larger and older.

2.2 Meteorological measurements and irrigation schedule

Hourly meteorological data were acquired by an automatic weather station located about 300 m from the plot and managed by DEMETER (Agrometeorological Service - www.meteo-agriculture.eu/qui-sommes-nous/lhistoire-de-demeter). These micrometeorological data were valuable to estimate the initial soil conditions and the changes in time (Figure 2). Potential evapotranspiration (ETP) was computed according to the Penman-Monteith formula accounting for the incoming short-wave solar radiation, air temperature, air humidity, wind speed and rainfall measured by the station. Prior to June 19, 2017, date of the first field data acquisition, little precipitation was recorded for 5 days (only 2.5mm on June 13) and only 18mm cumulative precipitation was recorded during the entire month of June 2017. The mean air temperature was very high (35°C under a well-ventilated shelter). Consequently, the plants were probably suffering from water deficit at the time of the experiment. Thus, at the start of the experiment, we assumed that the soil water content (SWC) around the plants was probably below field capacity. As shown in Figure 2, the evapotranspiration rate was about 5.6 mm/day.

The controlled infiltration experiment was conducted using a sprinkler installed between the two monitored plants, placed at an elevation of 1.4m, in order to apply irrigation water as uniformly as possible. The irrigation started on June 19, 2017 at 13h00 and ended two hours later (15h00) for a total of 260 liters (104 l/h). Runoff was observed due to topography and probably induced more water supply for plant A that is located downhill. The irrigation water had an electrical conductivity of 720µS/cm at 15°C.

2.3 ERT and MALM data acquisition

We carried out a time-lapse microscale ERT acquisition, based on custom-made ERT boreholes (six of them, each with 12 electrodes), plus surface electrodes. The six boreholes were placed to form two equal rectangles at the ground surface. Each rectangle size was 1 m by 1.2m respectively in the row and inter-row line directions, with a vine tree placed at the centre of each rectangle. The boreholes were installed in June 2015 and a good electrical contact with soil was already achieved at the time of installation. The topmost electrode in each hole was 0.1 m below ground, with vertical electrode spacing along each borehole equal to 0.1 m. In each rectangle, 24 surface electrodes surrounded the plant stem arranged in a five by five regular mesh (with one skipped electrode near the stem). We conducted the acquisitions on each rectangle independently. Each acquisition was therefore performed using 72 electrodes (24 surface and 48 electrodes in 4 boreholes) using an IRIS Syscal Pro resistivity meter. For all measurements we used a skip 2 dipole-dipole acquisition (i.e., a configuration where the current dipoles and potential dipoles are three times larger than the minimal electrode spacing).

In addition to acquiring ERT data, we also acquired MALM data. MALM acquisition was logistically the same as ERT and was support by the same device, but used a pole-pole scheme (with two remote electrodes). Borehole and surface electrodes composing the measurement setup were used as potential electrodes, while current electrode C1 was planted directly into the stem, 10 cm from the soil surface, with an insertion depth of about 2 cm, in order to inject current directly into the cambium layer. The two remotes electrodes C2 (for current) and P2 (for voltage) were placed approximatively at 30m distance from the

SOIL Discuss., https://doi.org/10.5194/soil-2019-28
Manuscript under review for journal SOIL
Discussion started: 22 May 2019

plot, in opposite directions. Note that for MALM (unlike than for ERT), one corner surface electrode was put near the stem in order to refine the information at the centre of each rectangle.

Each MALM acquisition was accompanied by a companion MALM acquisition where the current electrode C1 was placed directly in the soil next to the stem rather than in the stem itself. In this way the effect of the plant stem-root system in conveying current can be evidenced directly comparing the resulting voltage patterns resulting from the two MALM configurations.

For both ERT and MALM, we acquired both direct and reciprocal configurations (that swap current and voltage electrode pairs), in order to assess the reciprocal error as an estimate of measurement error (see e.g. Cassiani et al., 2006). We adopted a time-lapse approach, conducting repeated ERT and MALM acquisitions over time in order to assess the evolution of the system's dynamics under changing moisture conditions associated with the infiltration experiment. We conducted repeated measurements starting on 19 June 2017 at 10:20 LT, and ending the next day at about 17:00 LT. The schedule of the acquisitions and the irrigation times is reported in Table 1.

2.4 Data analysis and processing

2.4.1 Micro-ERT time lapse analysis

The inversion of ERT data was conducted using the classical Occam's approach (Binley and Kemna, 2005). We conducted both absolute inversions and time-lapse resistivity inversions, as done in other papers (e.g. Cassiani et al., 2015, 2016). We used for inversion only the data that pass the 10% reciprocal error criterion at all measurement times. We inverted the data using the R3t code (Binley, 2019) adopting a 3-D mesh with very fine discretization between the boreholes, while larger elements were used for the outer zone.

2.4.2 MALM modelling and source inversion

We measure the voltage V at N points, corresponding to the N electrodes locations, x_1, x_2, …, x_N. Voltage depends on the density of current sources C according to Poisson's equation:

$$\nabla \cdot (\sigma \nabla V) = C \quad (1)$$

where σ is the conductivity of the medium, here assumed to be defined by the conductivity distribution obtained from ERT data inversion. The main idea behind the source inversion is to identify the distribution of current sources $C(x,y,z)$ – in practice located at the mesh nodes $\boldsymbol{C}=[C_1, C_2, \ldots, C_{Ns}]$ – that produce the measured voltage V distribution in space. In general, given a distribution of current sources it is relatively straightforward to calculate the resulting V field, once $\sigma(x,y,z)$ is known from ERT inversion. Vice versa, the identification of $C(x,y,z)$ distribution given $V(x,y,z)$ and $\sigma(x,y,z)$ is an ill-posed problem, that requires regularization and/or a priori assumptions in order to deliver stable results. Different approaches are possible – for a detailed analysis in this context see Mary et al. (2018). In this paper we have used the simplest approach, i.e. we assumed that one single current source was responsible for the entire voltage distribution. For each candidate location the sum of squares

between computed and measured voltages was used as an index of "likelihood" of that location as a possible MALM current source in the ground. Mary et al. (2018) introduced a simple index that can be mapped in the three-dimensional soil space and that measures the "likelihood" that a specific location is the (single) current source generating the observed voltage field. This index (*F1*) is defined as:

$$F1(D_m, D_{f,i}) = \left\| D_m - D_{f,i} \right\|_2 \quad (2)$$

Where D_m is the measured voltage, and $D_{f,i}$ is the modelled voltage corresponding to a single source injecting the entire known injected current at the i-th node in the mesh. The forward modelling producing the $D_{f,i}$ values is based on the direct solution of the DC current flow in a heterogeneous medium, such as implement in the R3t Finite Element code (Binley, 2019). Thus the *F1* inversion accounts naturally for the heterogeneous electrical resistivity of the 3D soil volume, also in its evolution over time (e.g. as an effect of irrigation and RWU).

While more advanced attempts could be made (such as the *F2* approach also described by Mary et al., 2018) the simple *F1* approach is capable of imaging the likely location of current sources in the ground, that in turn represent - according to our key assumptions – the locations where roots have an active contact with the soil.

3 Results and discussion

3.1 Background and irrigation time steps of ERT measured data

The soil electrical conductivity during the period prior to the infiltration (see ERT results in Figure 2a and 2b, respectively for Plants A and B) ranged from 50 to 200 Ωm, with a median value around 100 Ωm, a range that is reasonable for a dry sandy soil. For plant A, i.e. the smaller plant, the highest resistivity values were distributed at about 0.5 m depth (Figure 3a), For the larger plant B (Figure 3c), the positive resistivity anomalies are more diffused and less intense (150 Ω.m) compared to plant A, which reach larger depths. The background time (T0) for both plants revealed a low resistive layer ranging from 0 to 0.35 m depth for plant A and to 0.25m for plant B. The first time step (T1) was collected during the irrigation, at 2h for plant A and at 30 minutes for plant B after the beginning of the irrigation. Figure 3b and Figure 3d show the resistivity distribution during irrigation (at time step T1). The input of low resistivity water (15 Ωm, measured in laboratory) caused a homogeneous drop of the resistivity values that make the two images around plant A and plant B very similar to each other, which is an indirect evidence that water infiltrated similarly in both areas (that are next to each other) with no difference in soil hydraulic properties. The very small-scale anomalies observed at the soil surface are likely to be caused by heterogeneous direct evaporation patterns or different soil compaction. More interesting are the resistive anomalies at intermediate depths. As observed in other case studies (e.g. Cassiani et al., 2015, 2016, Consoli et al., 2017; Vanella et al. 2018), these are likely to be linked to soil saturation decrease caused by RWU, particularly in consideration of its intensity during this time of the year (June) for non-irrigated crops. Of course, we cannot fully exclude that higher resistivity is also related to woody roots presence, especially when they are dense. Besides, roots could also have induced soil swelling creating voids acting like resistive heterogeneities. Consistently

SOIL Discuss., https://doi.org/10.5194/soil-2019-28
Manuscript under review for journal SOIL
Discussion started: 22 May 2019

to the age and size of plants, plant A that is smaller and younger is associated to an estimated root system that is shallower and more concentrated (Figure 3a) while plant B seems to have a root system deeper and larger (Figure 3c).

3.2 Background and irrigation time steps of MALM measured data

Figure 4 shows the raw results of MALM acquisition on plant A, during background and irrigation, for both soil and stem injection configurations. Note that voltages are normalized against the corresponding injected current. For both surface and borehole electrodes the normalized voltage distribution can be compared against the one expected from the solution for a point injection of current I at the surface of a homogeneous soil of resistivity ρ:

$$V = \frac{I\rho}{2\pi r} \tag{3}$$

where r is the distance between the (surface) injection point and the point where voltage V is computed (see Figure 4e for a comparison). In all cases, both for surface and borehole electrodes, and both for stem and soil current injection, the voltage patterns are deformed with respect to the solution of Eq. (3) for a homogeneous soil. Some pieces of evidence are apparent from the raw data already:

a. In all cases, the pattern of surface and subsurface voltage is asymmetric with respect to the injection point (in the stem or close to it, in the soil) and thus different from the predictions of Eq. (3); this indicates that current pathways are controlled by the soil heterogeneous structure: note that at all times there is a clear indication that a conductive pathway extends from the plant to the right-upper corner of the image (this would be the classical use of MALM – identifying the shape of conductive bodies underground). Note that spatial variations of voltage between boreholes are consistent with surface observations i.e. the maximum voltage was measured on the borehole 4 located in the top right corner of the plot;
b. The voltage patterns in the case of stem injection are clearly different from the corresponding ones obtained from soil injection. In particular, injecting in the soil directly produces a stronger voltage signal both at the surface and in the boreholes than the corresponding voltage in the case of stem injection: this difference clearly points towards the fact that the plant-roots system must convey the current in a different way than the soil alone; tentatively the observed voltage features would indicate a deeper current injection in the case of stem injection. Looking at the qualitative differences between soil and stem injection in the borehole electrode data, the impact is very small at depths larger than 0.6m;
c. For both soil and stem injection, local anomalies observed in the background image are either removed or smoothed during the irrigation steps. The effect is equally pronounced in soil and stem injection, showing that this is caused essentially by the change in resistivity induced by the change in soil water content (see Figure 3Figure 4).

Similar features are observed for plant B (results not shown for brevity).

Figure 4 shows the time evolution of normalized voltage values for both stem and soil injection for plant A. As apparent from the raw data in Figure 4, during irrigation all electrodes recorded a decrease of the normalized voltage. However, a consistent and quantitative interpretation is not straightforward by a visual inspection of the raw data (Figure 4, or similar data for Plant B).

3.3 Inversion of virtual current sources to estimate roots extents

Figure 6 shows the iso-surfaces of fitness index *F1* (Eq. 2) for the background (pre-irrigation) conditions of both plants A and B, and for current injection in the soil and in the stem at all-time steps listed in Table 1. In all cases, Figure 6 shows the iso-surface corresponding to the value *F1*= 7V corresponding to the 25% percentile (value selected after analysing the evolution of the curve of sorted misfit *F1*), thus the images provide comparable information for all cases. In particular, the inversion procedure highlights the remarkable difference, for both plants A and B, between the injection in the stem and in the soil. Current injection in the soil produces a voltage distribution that, albeit corresponding to a heterogeneous resistivity distribution and thus different from the predictions of a simpler model such as Eq. (3), collapses effectively to one point, i.e. the point where current was effectively injected in the ground. On the contrary, when current is injected in the stem, the region of possible source locations in the ground is much wider, and depicts a volume that is likely to correspond to the contact points between roots and soil, i.e. the volume where roots have an active role in the soil especially in terms of RWU. While this latter interpretation remains somewhat speculative, at least in the present experimental context, nevertheless the different results between soil and stem injection are absolutely apparent and can only find an explanation in the role of roots and their spatial structure.

The most interesting feature shown by Figure 6 is that the likely source volumes do not change with time during irrigation. Note that this inversion makes use of the changing electrical resistivity distributions caused by infiltrating water (see Figure 3) thus the result is not obvious, and indicates an underlying mechanism that is likely to be linked to the permanence of the roots structure over such a short time lapse.

3.4 Electrical resistivity variations inside and outside the likely active roots zone

As the changes in the estimated extent of the root zone are only minor (Figure 6), it makes sense to evaluate the changes, as an effect of irrigation, in electrical resistivity within such stable estimated root zone. Figure 7 shows the ER variations in the zones inside and outside this estimated active root zone. It is apparent how irrigation causes a general decrease of electrical resistivity for both plants A and B, and in both inner and outer regions. Note that even though the regions are different for the two plants, the behaviour is similar. Then at the end of irrigation we observe, for both plants, that resistivity continues to decrease outside the root active region, while it increases slightly inside. This behaviour is consistent with the fact that inside the region we expect that RWU progressively dries the soil, while outside this region resistivity continues to decrease (overall)

as an effect (probably) of water redistribution in the unsaturated soil. It must be noted that the relationships between resistivity and soil moisture content is non-linear (e.g. Archie, 1942; Waxman and Smits, 1968; Brovelli and Cassiani, 2011).

4 Conclusions

This study presents an approach to define the extent of active roots distribution using non-invasive investigations, and thus particularly suitable to be applied under real field conditions. We applied a mix of ERT and MALM techniques, using the same electrode and surface electrode distribution. The power of the approach lies in the complementary capabilities of the two techniques in providing information concerning the root structure and activity:

(a) ERT provides 3D high resolution images of electrical resistivity distribution in the subsoil housing the root system. Fast acquisition allows the measurement of resistivity changes over time, which in turn can be linked to changes in SWC. This can be caused e.g. by water infiltration, or by RWU: in the latter case, negative SWC changes mapped through resistivity changes can be used to map the regions where roots exert an active suction and reduce SWC. However, water redistribution in the soil also plays a role in terms of resistivity changes. Thus some additional independent information about the location of active roots in the soil may help: this is the first coupling between ERT and MALM.

(b) MALM, and particularly its double application of current injection in the stem and in the soil next to it, uses electrical measurements in a totally different manner: here the plant-root system itself acts as a conductor, and the goal is to use the retrieved voltage distribution to infer where the current injected in the stem actually is conveyed into the soil: these locations are potentially the same locations where roots interact with the soil in terms of RWU. However, in order to try and locate the position of these points, it is necessary to know the soil electrical resistivity distribution at the time of measurements. This can be provided by (time-lapse) ERT measurements: this is the second coupling between ERT and MALM.

The approach has been successfully tested in a vineyard during an irrigation experiment. The survey was carried out during a sunny summer season in a generally non-irrigated vineyard of the Bordeaux Region. The site is composed of sandy-loamy soil, thus there is a high infiltration rate during the experiment, and this would make it more difficult to distinguish RWU zones from infiltration zones as done for instance by Cassiani et al. (2015) using time-lapse ERT alone.

The key additional information is provided by MALM, and particularly by the simple inversion seeking for a single current injection point that we have adopted. This directly incorporates the ERT information in terms of changing electrical resistivity distribution in space including its evolution in time.

On one hand, this gives clear evidence that injecting current in the soil and in the stem produces different inversions. The soil injection leads practically to identifying the true single electrode location . The stem injection helps identify a 3D region of likely distributed current injection locations, thus defining a region in the subsoil where RWU is likely to take place.

The latter result is particularly useful, in perspective: when computing the time-lapse changes of electrical resistivity inside and outside this tentative RWU region during irrigation we clearly see that while inside resistivity increases (as an effect of RWU, as irrigation is still ongoing), outside resistivity decreases. Thus our assumption that the region identified by MALM inversion (albeit very rough) corresponds to the RWU region is corroborated indirectly also by this evidence.

The presented approach can be easily replicated under a variety of conditions, as DC electrical methods such as ERT and MALM do not possess a spatial scaling per se, but their resolution depends on electrode spacing as well as on other factors that are difficult to assess a priori, such as resistivity contrasts and signal to noise ratio. Thus similar experiments can also be used in the laboratory, where more direct evidence of root distribution can be used to further validate the method.

5 Acknowledgements

The authors wish to acknowledge support from the ERANET-MED project WASA ("Water Saving in Agriculture: Technological developments for the sustainable management of limited water resources in the Mediterranean area"). The authors from the University of Padua acknowledge support also from the University Research Project "Hydro-geophysical monitoring and modelling for the Earth's Critical Zone" (CPDA147114). In addition, the information, data or work presented herein was funded in part by the Department of Energy Advanced Research Projects Agency-Energy (ARPA-E) project under work authorization number 16/CJ000/04/08 and Office of Science Biological and Environmental Research Watershed Function SFA project under Contract Number DE-AC02-05CH11231. The views and opinions of authors expressed herein do not necessarily state or reflect those of the United States Government or any agency thereof. Luca Peruzzo and Myriam Schmutz gratefully acknowledge the financial support from IDEX (Initiative D'EXellence, France), the European regional development fund Interreg Sudoe – Soil Take Care, no. SOE1/P4/F0023 – Sol Precaire.

References

Amato, M. *et al.* Multi-electrode 3d resistivity imaging of alfalfa root zone. *Eur. J. Agron.* 31, 213–222 (2009).

Anderegg W.R.L, J.M. Kane and L.D.L. Anderegg, 2013, Consequences of widespread tree mortality triggered by drought and temperature stress, *Nature Climate Change*, 3(1), 30-36, doi: 10.1038/nclimate1635.

Archie, G. E. The electrical resistivity log as an aid in determining some reservoir characteristics. *Transactions AIME* 146, 54–62 (1942).

Band L.E., J.J. McDonnell, J.M. Duncan, A. Barros, A. Bejan, T. Burt, W.E. Dietrich, R.E. Emanuel, T. Hwang, G. Katul, Y. Kim, B. McGlynn, B. Miles, A. Porporato, C. Scaife, P.A. Troch, 2014, Ecohydrological flow networks in the subsurface, *Ecohydrology*, 7(4), 1073-1078, doi: 10.1002/eco.1525.

Binley, 2019, A. R3t version 1.9. *User Guide. University of Lancaster, UK.*

Binley, A. and A. Kemna, 2005, DC resistivity and induced polarization methods. In *Hydrogeophysics*, 129–156, Springer.

Brovelli A. and G. Cassiani, 2011, Combined estimation of effective electrical conductivity and permittivity for soil monitoring, *Water Resources Research*, 47, W08510, doi:10.1029/2011WR010487.

Brillante, L., Mathieu, O., Bois, B., van Leeuwen, C. and Lévêque, J.: The use of soil electrical resistivity to monitor plant and soil water relationships in vineyards, SOIL, 1(1), 273–286, doi:10.5194/soil-1-273-2015, 2015.

Campbell, R. B., Bower, C. A., and Richards, L. A., 1949, Change of Electrical Conductivity With Temperature and the Relation of Osmotic Pressure to Electrical Conductivity and Ion Concentration for Soil Extracts, Soil Sci. Soc. Am. J., 13, 66, doi: 10.2136/sssaj1949.036159950013000C0010x.

Cassiani, G., Bruno, V., Villa, A., Fusi, N. and A.M. Binley, 2006, A saline trace test monitored via time-lapse surface electrical resistivity tomography. *J. Appl. Geophys.* 59, 244 – 259, doi: 10.1016/j.jappgeo.2005.10.007.

Cassiani, G., Ursino, N., Deiana, R., Vignoli, G., Boaga, J., Rossi, M., Perri, M. T., Blaschek, M., Duttmann, R., Meyer, S., Ludwig, R., Soddu, A., Dietrich, P., and Werban, U., 2012, Noninvasive Monitoring of Soil Static Characteristics and Dynamic States: A Case Study Highlighting Vegetation Effects on Agricultural Land, Vadose Zone J., 11, 3, https://doi.org/10.2136/vzj2011.0195.

Cassiani, G., Boaga, J., Vanella, D., Perri, M. T. & Consoli, S. Monitoring and modelling of soil-plant interactions: the joint use of ert, sap flow and eddy covariance data to characterize the volume of an orange tree root zone. *Hydrol. Earth Syst. Sci.* 19, 2213–2225, DOI: 10.5194/hess-19-2213-2015 (2015).

Cassiani G., J. Boaga, M. Rossi, G. Fadda, M. Putti, B. Majone, A. Bellin, 2016, Soil-plant interaction monitoring: small scale example of an apple orchard in Trentino, North-Eastern Italy, *Science of the Total Environment*, Vol. 543, Issue Pt B, pp. 851-861, doi: 10.1016/j.scitotenv.2015.03.113.

Chahine M.T., 1992, The hydrological cycle and its influence on climate, *Nature*, 359, 373-380, doi: 10.1038/359373a0

Consoli S., F. Stagno, D. Vanella, J. Boaga, G. Cassiani, G. Roccuzzo, 2017, Partial root-drying irrigation in orange orchards: effects on water use and crop production characteristics, *European J. of Agronomy*, Volume 82, 190-202, doi: 10.1016/j.eja.2016.11.001.

Couvreur V., J. Vanderborght and M. Javaux, 2012, A simple three-dimensional macroscopic root water uptake model based on the hydraulic architecture approach, *Hydrol. Earth Syst. Sci.*, 16(8O, 2957-2971, doi: 10.5194/hess-16-2957-2012

Dalton, F. N., 1995, In-situ root extent measurements by electrical capacitance methods, Plant Soil, 173, 157–165, doi: 10.1007/BF00155527.

Dawson T.D. and R.T.W. Siegwolf (eds), 2007, Stable Isotopes as Indicators of Ecological Change, *Terrestrial Ecology Series*, *Elsevier*, 417 pp.

de Arellano J.V.G., C.C. van Heerwaarden, J. Levieveld, 2012, Modelled suppression of boundary-layer clouds by plants in a CO2-rich atmosphere, *Nature Geoscience*, 5(10), 701-704, doi: 10.1038/NGEO1554.

De Carlo L., M.T. Perri, M.C. Caputo, R. Deiana, M. Vurro and G. Cassiani, 2013, Characterization of the confinement of a dismissed landfill via electrical resistivity tomography and mise-à-la-masse, *Journal of Applied Geophysics*, 98 (2013) 1–10, doi: 10.1016/j.jappgeo.2013.07.010.

Dirmeyer P.A., R.D. Koster and Z. Guo, 2006, Do global models properly represent the feedback between land and atmosphere? , *J. of Hydrometeorology*, 7(6), 1177-1198, doi: 10.1175/JHM532.1.

Dirmeyer, P. A., E. K. Jin, J. L. Kinter III and J. Shukla, 2014: Land Surface Modeling in Support of Numerical Weather Prediction and Sub-Seasonal Climate Prediction. *White Paper*: Workshop on Land Surface Modeling in Support of NWP and Sub-Seasonal Climate Prediction, 17pp.

Draye X., Y. Kim, G. Lobet and M. Javaux, 2010, Model-assisted integration of physiological and environmental constraints affecting the dynamic and spatial patterns of root water uptake from soils, *J. of Experimental Botany*, 61(8), 2145-2155, doi: 10.1093/jxb/erq077.

Dupuy L., M. Vignes, B.M. McKenzie and P.J. White, 2010, The dynamics of root meristem distribution in the soil, *Plant, Cell and Environment*, 33(3), 358-369, doi: 10.1111/j.1365-3040.2009.02081.x.

Dupuy L., T. Fourcaud, A. Stokes and F. Danion, 2005, A density-based approach for the modelling of root architecture: application to Maritime pine (Pinus pinaster Ait.) root systems, *J. of Theoretical Biology*, 3, 323-334, doi: 10.1016/j.jtbi.2005.03.013.

Dupuy L. and M. Vignes, 2012, An algorithm for the simulation of the growth of root systems on deformable domains, *J. of Theoretical Biology*, 310, 164-174, doi: 10.1016/j.jtbi.2012.06.025.

Garré, S., Javaux, M., Vanderborght, J., Pagès, L. & Vereecken, H., 2011, Three-dimensional electrical resistivity tomography to monitor root zone water dynamics. *Vadose Zone J.* 10, 412–424 doi: 10.2136/vzj2010.0079.

Gerwitz A. and E.R. Page, 1974. Empirical Mathematical - Model to Describe Plant Root Systems 1. *Journal of Applied Ecology*, 11, 773-781.

Gibert, D., Le Mouël, J.-L., Lambs, L., Nicollin, F., and Perrier, F., 2006, Sap flow and daily electric potential variations in a tree trunk, Plant Sci., 171, 572–584, doi: 10.1016/j.plantsci.2006.06.012.

Hackett C. and D.A. Rose, 1972, A model of the extension and branching of a seminal root of barley, and its use in studying relations between root dimensions. I. The model. *Aust. J. Biol. Sci.*, 25, 669–679.

Jourdan C. and H. Rey, 1997, Modelling and simulation of the architecture and development of the oil-palm (Elaeis guineensis Jacq) root system .1. The model, *Plant and Soil*, 190(2), 217-233, doi: 10.1023/A:1004218030608

Kemna A., A. Binley, G. Cassiani, E. Niederleithinger, A. Revil, L. Slater, K. H. Williams, A. Flores Orozco, F.-H. Haegel, A. Hördt, S. Kruschwitz, V. Leroux, K. Titov, E. Zimmermann, 2012, An overview of the spectral induced polarization method for near-surface applications, *Near Surface Geophysics*, doi: 10.3997/1873-0604.2012027.

Mary, B., G. Saracco, L. Peyras, M. Vennetier, P. Mériaux and C. Camerlynck, 2016, Mapping tree root system in dikes using induced polarization: Focus on the influence of . *J. Appl. Geophys.* 135, 387 – 396, doi: https://doi.org/10.1016/j.jappgeo.2016.05.005.

Mary, B., F. Abdulsamad, G. Saracco, L. Peyras, M. Vennetier, P. Mériaux and C. Camerlynck 2017, Improvement of coarse root detection using time and frequency induced polarization: from laboratory to field experiments. *Plant Soil* 417, 243–259, doi: 10.1007/s11104-017-3255-4.

Mary, B., Peruzzo, L., Boaga, J., Schmutz, M., Wu, Y., Hubbard, S. S., and G. Cassiani, 2018, Small scale characterization of vine plant root water uptake via 3D electrical resistivity tomography and Mise-à-la-Masse method, *Hydrol. Earth Syst. Sci.* , doi: 10.5194/hess-22-5427-2018.

Maxwell R.M, F.K. Chow and S.J. Kollet, 2007, The groundwater-land-surface-atmosphere connection: Soil moisture effects on the atmospheric boundary layer in fully-coupled simulations, *Advances in Water Resour*ces, 30(12), 2447-2466, doi: 10.1016/j.advwatres.2007.05.018.

Manoli G., S. Bonetti, J.C. Domec, M. Putti, G. Katul and M. Marani, 2014, Tree root systems competing for soil moisture in a 3D soil-plant model, *Advances in Water Resour*ces, *66*, 32–42, doi: 10.1016/j.advwatres.2014.01.006.

Michot, D., Benderitter, Y., Dorigny, A., Nicoullaud, B., King, D., and Tabbagh, A., 2003, Spatial and temporal monitoring of soil water content with an irrigated corn crop cover using surface electrical resistivity tomography: soil water study using electrical resistivity, Water Resour. Res., 39, doi: 10.1029/2002WR001581.

Michot, D., Thomas, Z. and Adam, I.: Nonstationarity of the electrical resistivity and soil moisture relationship in a heterogeneous soil system: a case study, SOIL, 2(2), 241–255, doi:10.5194/soil-2-241-2016, 2016.

Osiensky, J.L., 1997. Ground water modeling of mise-a-la-masse delineation of contaminated ground water plumes. J. Hydrol. 197 (1–4), 146–165. doi: 10.1016/S0022-1694(96)03279-9.

Parasnis, D. S., 1967, Three-dimensional electric mise-a-la-masse survey of an irregular lead-zinc-copper deposit in central Sweden, *Geophys. Prospect.* 15, 407–437, doi: 10.1111/j.1365-2478.1967.tb01796.x.

Perri M.T., P. De Vita, R. Masciale, I. Portoghese, G.B. Chirico and G. Cassiani, 2018, Time-lapse Mise-á-la-Masse measurements and modelling for tracer test monitoring in a shallow aquifer, *Journal of Hydrology*, 561, 461-477, doi: 10.1016/j.jhydrol.2017.11.013

Philip J.R., 1966, Plant Water Relations: Some Physical Aspects, *Annual Review of Plant Physiology*, 17, 245-268.

Rhoades, J. D., Raats, P. A. C., and Prather, R. J., 1976, Effects of Liquid-phase Electrical Conductivity, Water Content, and Surface Conductivity on Bulk Soil Electrical Conductivity1, Soil Sci. Soc. Am. J., 40, 651, doi: 10.2136/sssaj1976.03615995004000050017x.

Srayeddin, I. and Doussan, C., 2009, Estimation of the spatial variability of root water uptake of maize and sorghum at the field scale by electrical resistivity tomography, Plant and Soil, 319, 185–207, doi: 10.1007/s11104-008-9860-5, 2009.

Vanella D., G. Cassiani, L. Busato, J. Boaga, S. Barbagallo, A. Binley, S. Consoli, 2018, Use of small scale electrical resistivity tomography to identify soil-root interactions during deficit irrigation, *Journal of Hydrology*, 556, 310-324, doi: 10.1016/j.jhydrol.2017.11.025.

Volpe V., M. Marani, J.D. Albertson and G. Katul, 2013, Root controls on water redistribution and carbon uptake in the soil-plant system under current and future climate *Adv Water Resour*, 60, 110-120, doi: 10.1016/j.advwatres.2013.07.008.

York L.M., A. Carminati, S.J. Mooney, K. Ritz and M.J. Bennett, 2016, The holistic rhizosphere: integrating zones, processes, and semantics in the soil influenced by roots, *J. Exp. Botany*, 67(12), 3629-3643, doi: 10.1093/jxb/erw108.

Waxman, M. H. and Smits, L. J. M., 1968, Electrical Conductivities in Oil-Bearing Shaly Sands, Soc. Petrol. Eng. J., 8, 107–122, doi: 10.2118/1863-A.

Weigand, M. and Kemna, A.: Multi-frequency electrical impedance tomography as a non-invasive tool to characterize and monitor crop root systems, Biogeosciences, 14(4), 921–939, doi:10.5194/bg-14-921-2017, 2017.

Weigand, M. & Kemna, A., 2019, Imaging and functional characterization of crop root systems using spectroscopic electrical impedance measurements. *Plant and Soil*, 435(1-2), 201-224, doi: 10.1007/s11104-018-3867-3.

Werban, U., Attia al Hagrey, S., and Rabbel, W., 2008, Monitoring of root-zone water content in the laboratory by 2-D geo-electrical tomography, J. Plant Nutr. Soil Sc., 171, 927–935, doi: 10.1002/jpln.200700145.

SOIL Discuss., https://doi.org/10.5194/soil-2019-28
Manuscript under review for journal SOIL
Discussion started: 22 May 2019

Table 1: schedule of the acquisitions and the irrigation times; Plant A and B are measured consecutively and consist each time of three measurements: ERT, MALM stem and MALM soil.

Acquisition no.	Plant	Starting time (LT)	Ending time (LT)	Irrigation	Date
0 (background)	A	10:20	11:00		Day 1 (19 June 2017)
	B	12:20	13:00		
1 (Irrigation)	A	15:00	15:30	13h00 to 15h30, 104lh-1 For both plants	
	B	13:30	14:00		
2	A	17:00	17:30		
	B	18:00	18.45		
3	A	10:30	11:00		Day 2
	B	9:30	10:00		
4	A	14:00	14:30		
	B	15:00	15:30		
5	A	18:00	18:30		
	B	17:00	17:30		

SOIL Discuss., https://doi.org/10.5194/soil-2019-28
Manuscript under review for journal SOIL
Discussion started: 22 May 2019

458
459 **Figure 1: picture of the field site in May 2017 (a) wired plants investigated (b) and grape status during the experiment in June**
460 **2017 (c)**

461

SOIL Discuss., https://doi.org/10.5194/soil-2019-28
Manuscript under review for journal SOIL
Discussion started: 22 May 2019

462

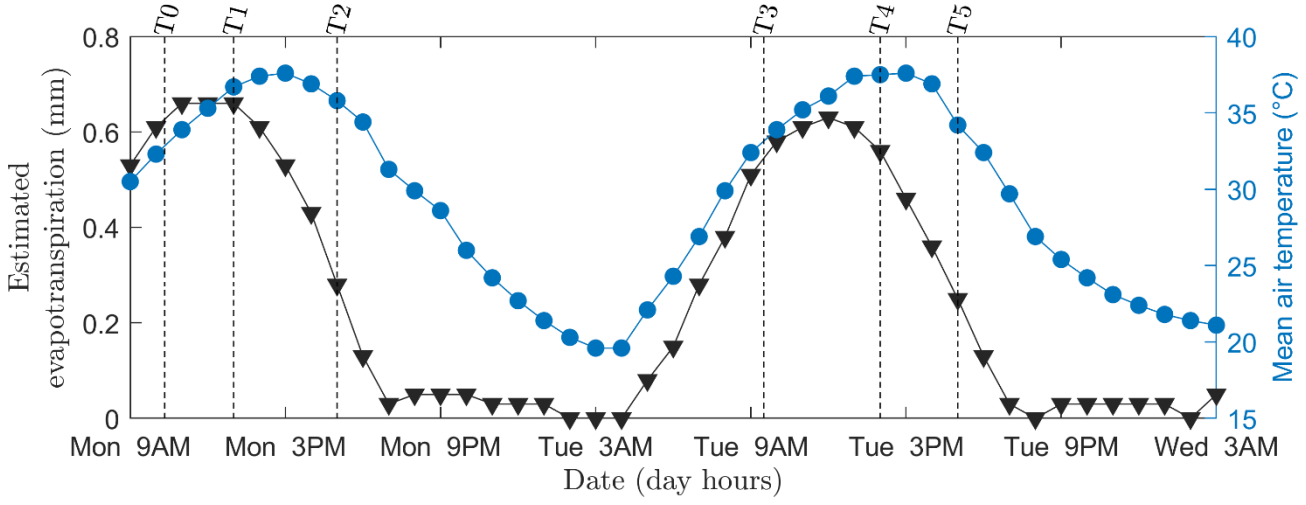

463

464 **Figure 2: variation of temperature (blue line) and estimated evapotranspiration (black line) derived from a nearby meteorological**
465 **station, during the 2-day irrigation experiment. The dashed vertical lines indicate acquisition times (see Table 1).**

SOIL Discuss., https://doi.org/10.5194/soil-2019-28
Manuscript under review for journal SOIL
Discussion started: 22 May 2019

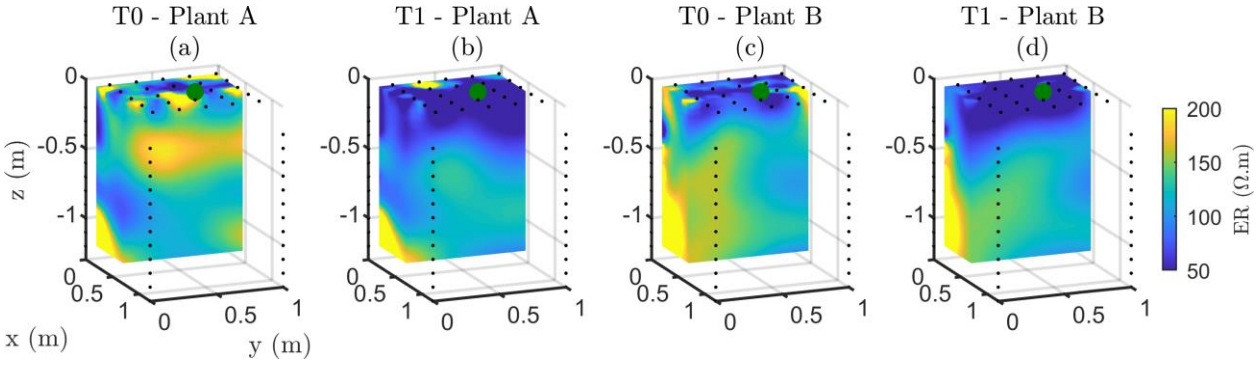

Figure 3: ERT results showing the 3D variations of electrical resistivity (in Ωm) for the initial state background T0 (a,c) and during irrigation T1 (b,d), for both plants A and B. The green point shows the positions of the plant stem.

SOIL Discuss., https://doi.org/10.5194/soil-2019-28
Manuscript under review for journal SOIL
Discussion started: 22 May 2019

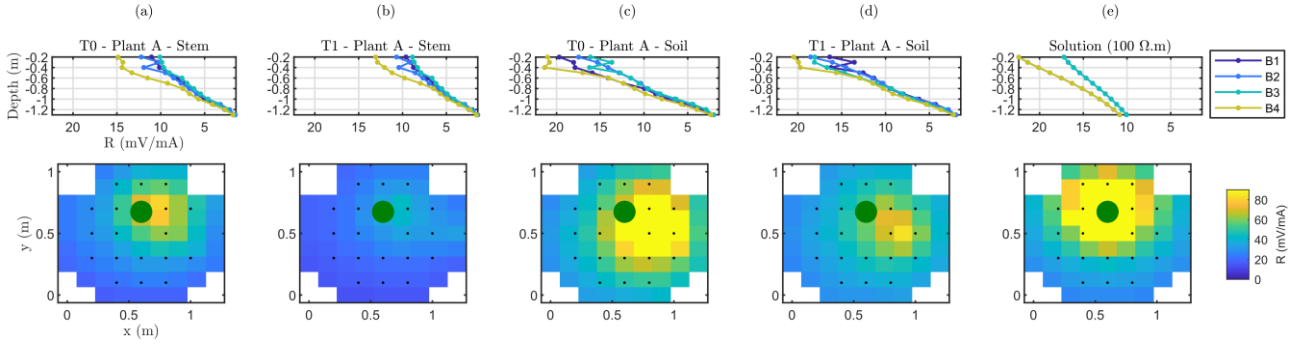

Figure 4: plant A, MALM results showing variations in surface (horizontal plan) of resistance R (in mV/mA) for the initial state background T0 (a,c) and irrigation T1 (b,d) time steps. Comparison between the stem injection (a,b) and soil injection (c,d). The black points show the surface electrodes location. The green point shows the positions of the plant stem. Data are filtered using a threshold on reciprocal acquisition of 20%. (e) shows the solution using eq. (2) for a homogeneous soil of 100 Ohm.m; The resistance between boreholes B1/B3 and B2/B4 are identical and cannot be distinguished graphically in the case of (e).

SOIL Discuss., https://doi.org/10.5194/soil-2019-28
Manuscript under review for journal SOIL
Discussion started: 22 May 2019

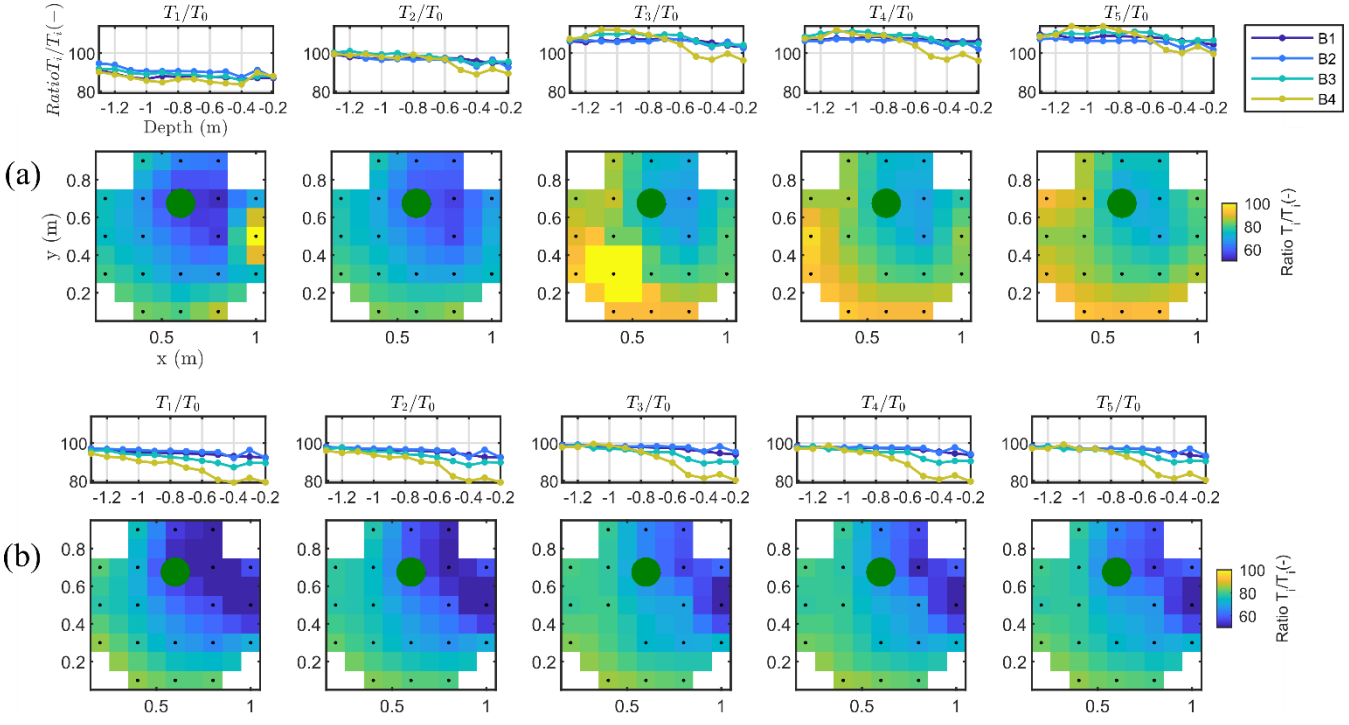

Figure 5: normalized voltage ratios (unitless) between time dataset Ti and T0 (T_i/T_0), measured for plant B. Above each plan view plot are the normalized voltage data measured using the boreholes electrodes, while map plots show ratios of normalized voltages measured with surface electrodes. Comparison between injection within (a) the stem (lines 1 and 2) and (b) in the soil (lines 3 and 4). The green point shows the positions of the plant stem.

SOIL Discuss., https://doi.org/10.5194/soil-2019-28
Manuscript under review for journal SOIL
Discussion started: 22 May 2019

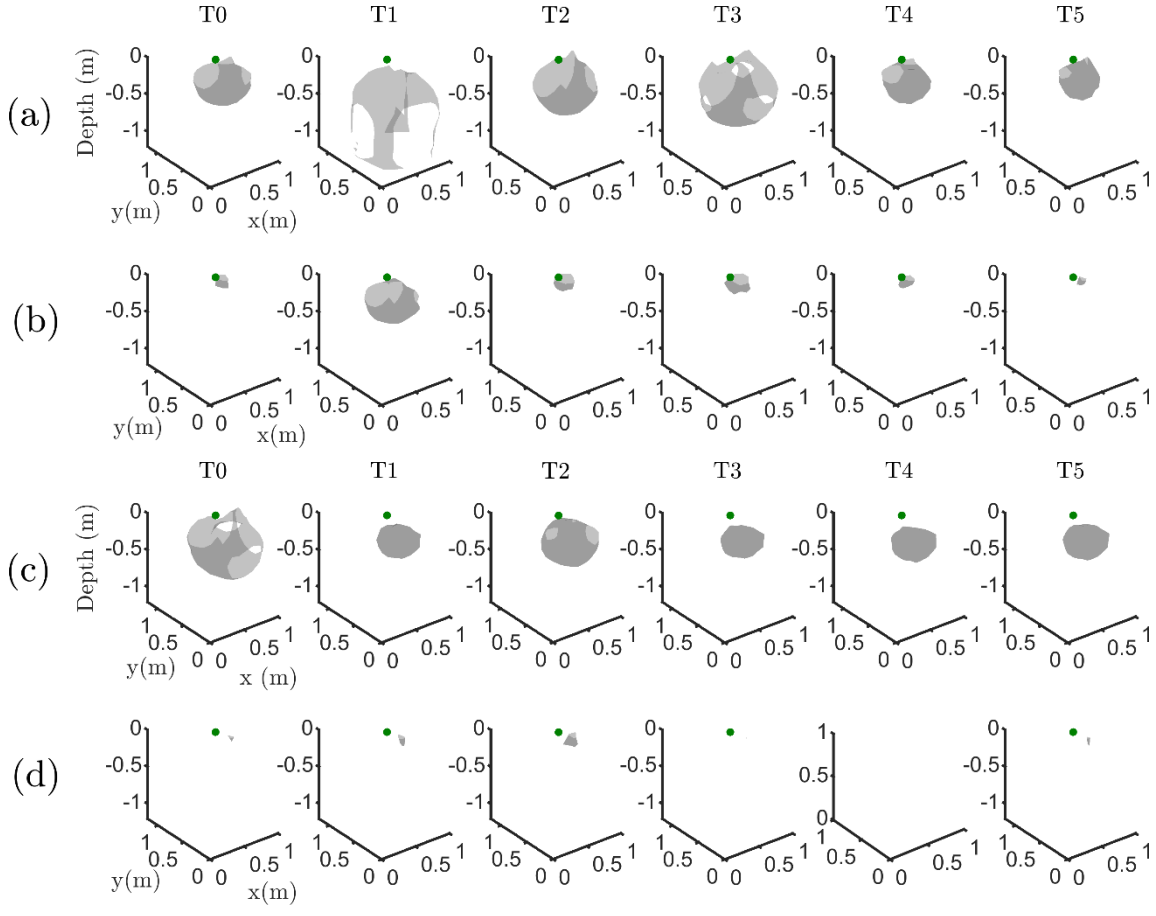

Figure 6: isosurface minimizing the *F1* function for plant B (a,b) and plant A (c,d); during stem injection (a,c), during soil injection (b,d); Columns represent the six times steps from T0 to T5. Green dot shows plant stem position. Threshold is defined by the percentile 25% of the normalised F1 (value selected according to the evolution of the curve of sorted misfit F1 and calculated for the tree injection at T0 and kept constant for all the time steps).

SOIL Discuss., https://doi.org/10.5194/soil-2019-28
Manuscript under review for journal SOIL
Discussion started: 22 May 2019

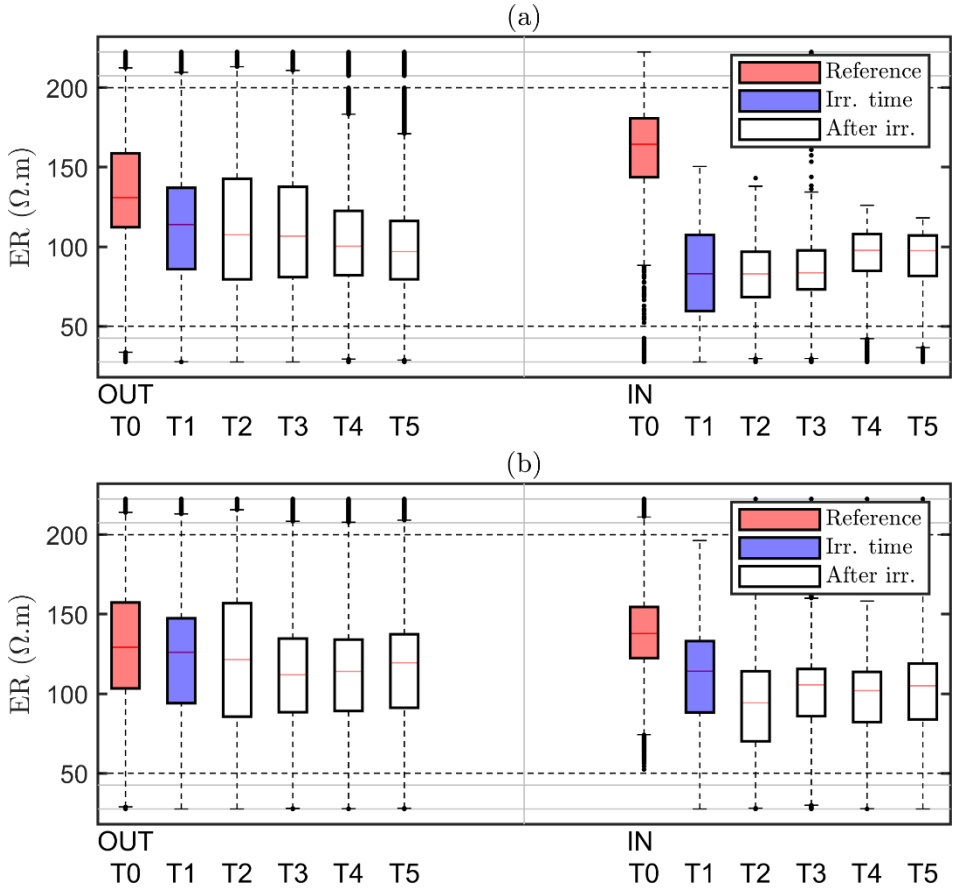

Figure 7: boxplot distribution of ER time variations observed on the plant A (top) and plant B (bottom), outside (OUT) of the region defined by the F1 best fit sources (see Fig. 6a-T0). The central mark indicates the median, the bottom and top edges of the box indicated the 25th and 75th percentiles of ER data, respectively. The whiskers extend to the most extreme data points not considered outliers.